

Brain tumor-targeted delivery and therapy by focused ultrasound introduced doxorubicin-loaded cationic liposomes

Qian Lin^{1,2} · Kai-Li Mao¹ · Fu-Rong Tian¹ · Jing-Jing Yang¹ · Pian-Pian Chen¹ · Jie Xu¹ · Zi-Liang Fan¹ · Ya-Ping Zhao² · Wen-Feng Li³ · Lei Zheng³ · Ying-Zheng Zhao¹ · Cui-Tao Lu^{1,2}

Received: 2 October 2015 / Accepted: 16 November 2015 / Published online: 14 December 2015
© Springer-Verlag Berlin Heidelberg 2015

Abstract Brain tumor lacks effective delivery system for treatment. Focused ultrasound (FUS) can reversibly open BBB without impacts on normal tissues. As a potential drug carrier, cationic liposomes (CLs) have the ability to passively accumulate in tumor tissues for their positive charge. In this study, FUS introduced doxorubicin-loaded cationic liposomes (DOX-CLs) were applied to improve the efficiency of glioma-targeted delivery. Doxorubicin-loaded CLs (DOX-CLs) and quantum dot-loaded cationic liposomes (QD-CLs) were prepared using extrusion technology, and their characterizations were evaluated. With the advantage of QDs in tracing images, the glioma-targeted accumulation of FUS + CLs was evaluated by fluorescence imaging and flow cytometer. Cell survival rate, tumor volume, animal survival time, and brain histology in C6 glioma model were investigated to evaluate the glioma-targeted delivery of FUS + DOX-CLs. DOX-CLs and QD-CLs had suitable nanoscale sizes and high entrapment

efficiency. The combined strategy of FUS introduced CLs significantly increased the glioma-targeted accumulation for load drugs. FUS + DOX-CLs showed the strongest inhibition on glioma based on glioma cell in vitro and glioma model in vivo experiments. From MRI and histological analysis, FUS + DOX-CLs group strongly suppressed the glioma progression and extended the animal survival time to 81.2 days. Among all the DOX treatment groups, FUS + DOX-CLs group showed the best cell viability and highest level of tumor apoptosis and necrosis. Combining the advantages of BBB reversible opening by FUS and glioma-targeted binding by CLs, ultrasound introduced cationic liposomes could achieve glioma-targeted delivery, which might be developed as a potential strategy for future brain tumor therapy.

Keywords Cationic liposomes · Focused ultrasound · Quantum dots · Doxorubicin · Glioma-targeted delivery

Electronic supplementary material The online version of this article (doi:10.1007/s00280-015-2926-1) contains supplementary material, which is available to authorized users.

✉ Ying-Zheng Zhao
pharmtds@163.com

✉ Cui-Tao Lu
lctuaa@163.com

¹ Present Address: College of Pharmaceutical Sciences, Wenzhou Medical University, Wenzhou 325035, Zhejiang Province, China

² Present Address: The Second Affiliated Hospital of Wenzhou Medical University, Wenzhou 325000, Zhejiang Province, China

³ The First Affiliated Hospital of Wenzhou Medical University, Wenzhou 325000, Zhejiang Province, China

Abbreviations

DOX	Doxorubicin
CLs	Cationic liposomes
FUS	Focused ultrasound
MRI	Magnetic resonance images
DOX-CLs	Doxorubicin-loaded cationic liposomes
QD	Quantum dots
QD-CLs	QD-loaded cationic liposomes

Introduction

Glioma is one of the most common primary brain tumors, which is classified into I–IV malignant grades based on the extent of cell proliferation, angiogenesis, and necrosis [1]. The annual incidence of glioma is growing gradually and

reaches to 2.4–7.0 per 100,000 in recent years [2, 3]. Even though aggressive therapies (such as surgery, chemotherapy, and radiotherapy) have been widely used, the recurrence and mortality rates of glioma are still high [4].

Though many active chemotherapeutics have been developed, they are not suitable for the treatment for malignant brain tumors due to the blood–brain barrier (BBB). Doxorubicin (DOX), also called adriamycin, is one of the most frequently used anticancer drugs. DOX has been successfully used to treat different solid and hematopoietic cancers such as breast cancer, osteosarcomas, aggressive lymphomas, and leukemias. From many previous researches, DOX also showed effective inhibition on glioma cells in both *in vitro* [5] and *in vivo* experiments [6, 7]. However, the limited survival advantage attributed to chemotherapy (i.e., DOX) is partially due to low central nervous system (CNS) penetration of anti-neoplastic agents across BBB [8]. Therefore, novel strategies are needed not only to open BBB with noninvasive method but also promote the action for cytotoxic drugs.

Previous studies demonstrated that low-power focused ultrasound (FUS) combined with a systemic injection of lipid- or polymer-shelled microbubbles could induce a non-invasive, local, and transient disruption on BBB [9–13]. Being constrained to the vasculature, ultrasonic microbubbles can interact strongly with low-intensity FUS and produce mechanical forces on the endothelium, which may result in transient disassembly of tight junctional complexes and the induction of active transport processes [14, 15]. With a phased transducer array and correction factors derived from computed tomography (CT) scans, FUS can be used to cross the skull without invasive craniotomy [16, 17]. When guided by magnetic resonance imaging (MRI), FUS could target precise anatomic structures in a completely noninvasive manner [18].

Some tumor cells were found to change their surface charges accompanied with their mutation in structure and functions during its malignant transformation [19]. To explore a “multistage targeting” strategy on glioma therapy, we focus on the cell surface charge to develop new drug carrier system. Cationic liposomes (CLs) have the potential to carry drugs [20]. CLs have the ability to passively accumulate in tumor tissues for their positive charge. This process, termed as “passive targeting,” can result in significant accumulation for loaded drugs, compared with the administration of free drug [21–23].

Quantum dots (QDs) have been widely studied for tumor-targeted imaging *in vitro*. Due to the nanoscale (2–10 nm), high selectivity, versatility, photostability, and capacity to get into cells or organelles via surface motility and oligomerization [24], QDs have attracted tremendous attention.

This study aims at developing a multistage targeting strategy for glioma chemotherapy—FUS-mediated technique combined with DOX-loaded CLs

(FUS + DOX-CLs), in which FUS induced BBB opening and CLs enhance the glioma-targeted delivery for DOX. In addition, QDs and magnetic resonance images (MRI) were used to evaluate the glioma-targeted efficiency and chemotherapeutic effect of the novel combined strategy. Glioma rat models were constructed to investigate the promoted glioma inhibition under FUS + DOX-CLs treatment. The feasibility of DOX-loaded cationic liposomes for ultrasound-triggered brain delivery on C6 glioma brain model was evaluated in this paper (as summarized in Fig. 1).

Materials and methods

Preparation of DOX-CLs and QD-CLs

CLs were composed of HSPC/DOPE/Chol/CTAB/Didodecyldimethylammonium bromide (10:1:3:5:2, wt/wt). CLs were prepared via extrusion technology and subsequent loading using ammonium sulfate method [25].

Lipids were dissolved in dehydrated ethanol at 65 °C. Liposomes were formed by injecting the lipid mixtures to 250 mM (NH₄)₂SO₄ solution (adjust pH to 5.5). The large unilamellar vesicles were sized by extrusion through 100-nm (five passes) and 50-nm (eight passes) polycarbonate membrane. The resulting vesicles had mean diameters ranging between 75 and 150 nm. Ethanol and nonencapsulated (NH₄)₂SO₄ were removed by dialysis method with 10 % sucrose solution (pH 5.5).

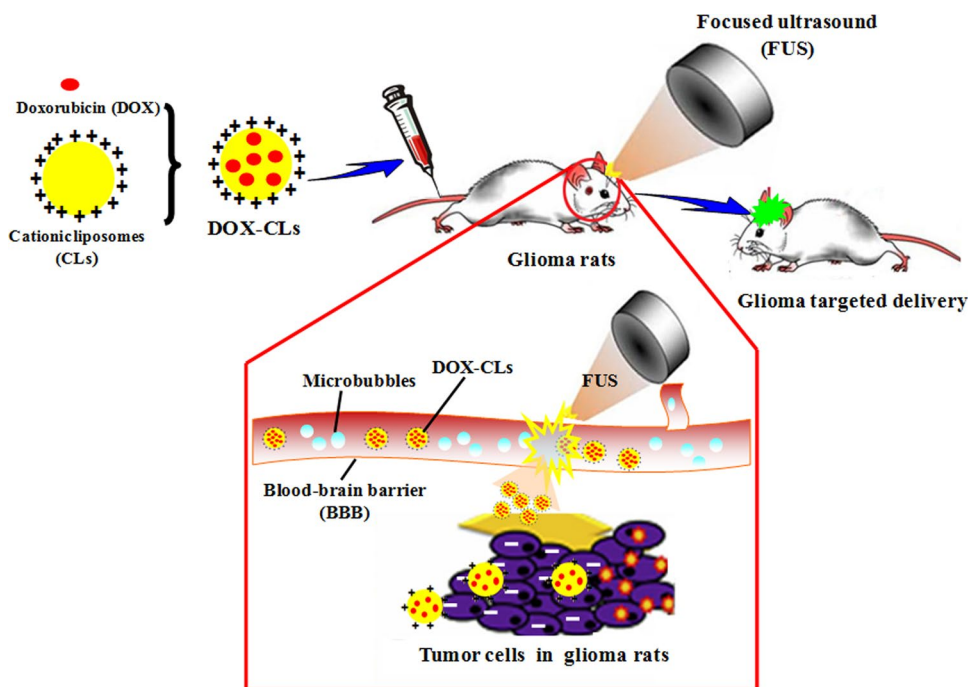
To evaluate the glioma-targeted efficiency of QDs combined with FUS, QDs were used as the model drug for DOX *in vivo*. To prepare DOX-CLs and QD-CLs, DOX and QD were added into blank liposome solution and incubated for 1 h at 65 °C, and then stored at 4 °C for 24 h.

Characterization of DOX-CLs and QD-CLs

The size and zeta potential values of blank lip, DOX-CLs, and QD-CLs were determined by a Zeta Potential/Particle Sizer Nicomp™ 380 ZLS (PSS. Nicomp, Santa Barbara, CA, USA). The pH of DOX-CLs suspension used for zeta potential analysis was 7.0.

To evaluate DOX-CLs encapsulation efficiency, DOX-CLs was separated from the nontrapped free DOX by Sephadex G-50 column. The effluent liquid containing DOX-CLs was collected and lyophilized at 5×10^{-4} Pa pressure for 20 h. Then, DOX-CLs lyophilized products were solved in anhydrous alcohol. The content of DOX was determined by HPLC (Kromasil C18, methanol/water = 75:25, velocity = 1.0 ml/min, detected wave length = 480 nm). Each sample was analyzed in triplicate. Entrapment efficiency was calculated with the following equation:

Fig. 1 Schematic diagram of brain tumor-targeted delivery by ultrasound introduced cationic liposomes



Encapsulation efficiency (%)

$$= \frac{\text{Encapsulated amount of DOX in CLs}}{\text{Total amount of DOX}} \times 100$$

To confirm uniformity and stability, all physical and chemical properties of QD-CLs were characterized by dynamic laser light scattering (Malvern Nano ZS-90 system Uniphase, San Jose, CA). QDs and QDs-CLs were observed by electron microscope. The emission peak of CdSeTe/ZnS core/shell QDs is approximately 800 nm (Invitrogen, OR, USA). The fluorescence property of QD-CLs, such as absorption spectrum, PL spectrum, and morphology, was evaluated under the fluorescence microscope (Nikon ECLIPSE 80i, Ruikezhongyi Company, Beijing, China). The entrapment efficiency of QD-CLs was measured by the fluorescence microscope.

Encapsulation efficiency (%)

$$= \frac{\text{Total amount of QDs} - \text{The amount of QDs in supernatant}}{\text{Total amount of QDs}} \times 100.$$

Glioma-targeted delivery by FUS introduced QD-CLs in vitro

Cell culture

C6 glioma cells were obtained from Cell Bank of the Chinese Academy of Sciences (Shanghai, China), cultured in DMEM high-glucose medium (4.5 g/L, Gibco, NY, USA) that was supplemented with 10 % fetal bovine serum (FBS, Gibco, NY, USA) and 1 % penicillin–streptomycin at pH

7.4. The cells were cultured in a humidified incubation chamber with 5 % CO₂ at 37 °C and were harvested with trypsin solution in their logarithmic growth phase for the following experiments.

In vitro fluorescence imaging of QD-CLs

The innate fluorescence of QDs allowed us to trace the localization of QDs in the cell. The C6 rat glioma cell line was cultured in 12-well plates overnight and then treated with QDs solution, QD-CLs, and FUS + QD-CLs at different concentrations, (50 and 100 nmol of QDs in QD-CLs) for 2 h at 37, respectively. Ultrasonic treatment performed after half-hour incubation under optimal conditions resulted from previous experiments. After the treatment, the cells were washed with PBS and imaged under a NIKON fluorescence microscope.

Cellular uptake of QDs

The efficiency of cellular uptake of QD in C6 cells was measured by flow cytometer (FACS Calibur FCM, Becton–Dickinson, San Jose, CA). C6 cells were seeded at a density of 2.5×10^4 per well on coverslips in 6-well plates. After incubated overnight at 37 °C, these 6-well plates were placed in 0.1 % FBS supplemented medium for 24 h and then incubated with QDs solution and QD-CLs, respectively (QDs concentration = 50 and 100 nmol) for another 48 h. FUS + QD-CLs group was experimented to observe whether FUS could enhance the endocytosis of QD-CLs. FUS treatment was performed after half-hour incubation under optimal

conditions resulted from previous experiments. The cells were then carefully washed three times by pre-warmed PBS, fixed in 4 % paraformaldehyde, and detached by 0.025 % trypsin/EDTA. The detached cells were collected into a flow cytometer to determine their uptake of the QD.

Glioma-targeted delivery by FUS introduced QD-CLs in vivo

FUS equipment

The experimental setup for FUS treatment is shown in Fig. 1. The focused ultrasound transducer (Acuson Sequoia 512C system, Siemens) was mounted in a three-dimensional positioning system and submerged in a tank filled with deionized water. The rat was placed on a tray below the water tank. A thin plastic water bag was placed between the rat brain and water tank for acoustic coupling. The efficacy of focused ultrasound-induced BBB disruption will be observed on C6 glioma rats. Pulsed ultrasound was focused in and around the tumor (frequency = 690 kHz, acoustic power = 0.32 W, burst length = 10 ms, repetition frequency = 1 Hz, duration = 60 s) with simultaneous IV administration of microbubble contrast agent. The equipment is summarized as Fig. 1.

Construction of glioma model

Consent and approval for this investigation were obtained from the Laboratory Animal Ethics Committee of Wenzhou Medical College and Laboratory Animal Centre of Wenzhou Medical College (Wenzhou, Zhejiang, China). Rats were provided by the Laboratory Animal Centre of Wenzhou Medical College.

Adult male Sprague–Dawley (SD) rats (200–220 g, China) were housed in an animal facility and maintained in a temperature- and light-controlled environment with an alternating 12-h light/dark cycle. Glioma rat model was induced by stereotactic injection of C6 cells following a previously reported procedure (16) with some modifications. Briefly, C6 cells were harvested and re-suspended for intracranial implantation. SD rats were anesthetized by an intraperitoneal injection of chloral hydrate (350 mg/kg body weight) and placed in a stereotactic head frame, and a small right frontal craniectomy was drilled 3 mm from the midline and 1 mm anterior to bregma. C6 cells ($1 \times 10^6/10 \mu\text{l}$) were implanted stereotactically to a depth of 5 mm below the craniectomy using a microinjection syringe. The craniectomy was resealed with bone wax, the skin was sutured together, and the rats were allowed to recover.

In vivo imaging of FUS introduced QD-CLs

To trace QD-CLs glioma-targeted effect, glioma fluorescence imaging was performed on 7, 13, and 25 days after QD-CLs injection in vivo. The rats were anesthetized with intraperitoneal injection of chloral hydrate 5 min before the experiment. The hair of the cranium was shaved with clippers. A 20-gauge cannula was inserted into the tail vein, and QD-CLs solution (50 nmol of QDs in QD-CLs) mixed with ultrasound microbubbles (300 $\mu\text{l}/\text{kg}$, 1×10^8 – 5×10^8 bubbles/ml) (SonoVue, Bracco International, the Netherlands) was infused. FUS was generated by a linear array transducer (14 MHz, Acuson Sequoia 512C system, Siemens). The linear array transducer was placed on the skull of the hemisphere at the locations of tumor cell implantation as well as the contralateral normal hemisphere. The parameters of the transducer sonication in the experimental group were set as follows: pulse repetition frequency of 1 Hz, sonication time of 60 s, burst length of 10 ms with acoustic power of 3 W. Four hours later, all animals were deeply anesthetized with chloral hydrate and infused with saline through the cardiac ventricle until colorless infusion fluid was obtained from the atrium. The brains were separated along the transverse suture and then imaged. The Maestro in vivo optical imaging system (CRI, Inc., US) was used for acquiring the fluorescence from the brains. The red filter set was applied, and image cube files were taken in series while scanning the liquid crystal filter from 500 to 700 nm (with 10-nm step). The fluorescent images were then analyzed by the vendor software.

To further confirm the in vivo imaging of FUS + QD-CLs, different sections of brains after fluorescence detection were processed with standard fixation and embedded in paraffin. According to the standard procedures, all paraffin-embedded specimens were cut and stained by Hoechst and HE.

Glioma inhibition by FUS introduced DOX-CLs in vitro and in vivo

Cancer cytotoxicity test

Anticancer activity of DOX in DOX-CLs and FUS + QD-CLs was evaluated with MTT assay on C6 glioma cells. The cells were grown in 96-well plate at 7000 cells per well under standard cell culture conditions for 24 h; further incubated in 0.1 % FBS supplemented medium for additional 24 h, and treated with DOX, DOX-CLs, and FUS + QD-CLs (DOX dose was 1 mg) for 72 h. The number of viable cells was determined by adding 20 μl of MTT (5 mg/ml) to each well and incubating for 4 h. After removal of the

Table 1 Experimental design of C6 glioma rats in vivo

Group	Treatment						
	C6 rats	Sham rats	saline	DOX	DOX-CLs	FUS	FUS + DOX-CLs
1 Control group (<i>n</i> = 10)	✓		✓				
2 DOX group (<i>n</i> = 10)	✓			✓			
3 DOX-CLs group (<i>n</i> = 10)	✓				✓		
4 FUS group (<i>n</i> = 10)	✓					✓	
5 FUS + DOX-CLs group (<i>n</i> = 10)	✓						✓

medium, 100 μ l dimethyl sulfoxide (DMSO) was added to each well. The absorbance was measured at 570 nm after 10-min incubation at room temperature.

Experiment design

To verify the treatment efficacy of DOX-CLs combined with FUS, 50 glioma rats were randomly divided into five groups as shown in Table 1. DOX in all groups was administered by intravenous injection twice weekly for a total of eight injections in 28 days. DOX-CLs were administered prior to US treatment. DOX dose in DOX-CLs, FUS + DOX-CLs, or DOX solution group was 5.67 mg/kg. C6 rats were anesthetized with chloral hydrate (350 mg/kg bodyweight) 5 min before the experiment. Treatment solution was infused via tail vein through a 20-gauge cannula. A linear array transducer (Acuson Sequoia 512C system, Siemens) was applied to generate the FUS effect. In the groups with FUS, the linear array transducer was placed over the tumor to blast the PMB (MI = 1.9, exposure time = 10 s).

Toxicity of FUS introduced DOX-CLs in vivo

For the toxicity evaluation, the normal SD rats were administered with DOX-CLs (17.01 mg/kg DOX dose in DOX-CLs) through tail vein injection. One month after the DOX-CLs injection and FUS, the SD rats were terminated, and the tissues from the major organs (heart, liver, spleen, lung, and kidney) were harvested and processed with HE staining for histological studies.

Tumor volume monitoring

To further assess the glioma inhibition effect of FUS + DOX-CLs, the tumor volume monitoring was performed weekly after the treatment by MRI. Animals were anesthetized with chloral hydrate (350 mg/kg) 5 min before MRI procedure.

All MRI images were acquired on a 3T scanner (Trio with Tim, Siemens, Erlangen, Germany) using the standard

wrist coil (Chenguang Medical Technologies Company, Shanghai, China) with an inner diameter of 13 cm. The tumor location was determined by performing a gradient echo FLASH sequence to acquire T1W images with the following imaging parameters: pulse repetition time (TR)/echo time (TE) = 560/27 ms; NEX = 2; matrix size = 256 \times 256; FOV = 56 mm \times 70 mm; slice thickness = 2.4 mm; slice spacing = 2.9 mm. Tumor size of animals in experiment group was quantified using turbo-spin-echo-based T2-weighted images with the following parameters: pulse repetition time (TR)/echo time (TE) = 2300/110 ms; NEX = 2; matrix size = 256 \times 256; FOV = 56 mm \times 70 mm; slice thickness = 2.4 mm; slice spacing = 2.9 mm.

To achieve enhanced T1-weighted and enhanced T2-weighted images, gadopentetate dimeglumine (Gd-DTPA, 0.4 mmol/kg) MRI contrast agent (Magnevist, Berlex Laboratories, Wayne, NJ) was administered as intraperitoneal injection 10 min before scanning.

Histology of brain tumors (HE)

Rat brain tumors were separated and fixed in 10 % buffered formalin, embedded in paraffin, and sectioned into 5 μ m thickness. Sections were stained with hematoxylin–eosin (H&E) to evaluate tumor progress. Under an optical microscope (Nikon ECLIPSE Ti-S, Ruikezhongyi company, Beijing, China), the tumor histology was viewed and imaged.

Apoptosis assay (TUNEL)

DNA fragmentation in situ was analyzed using the modified terminal deoxynucleotidyl transferase-mediated dUTP nick end-labeling (TUNEL) assay (Boster biological engineering Co., Wuhan, China) following the manufacturer's instructions. Cell staining and morphology were recorded by an optical microscope (Nikon ECLIPSE Ti-S, Ruikezhongyi Company, Beijing, China). The number of apoptotic tumor cells was evaluated by counting stained and featured apoptotic cells in four random microscopic fields (400 \times original magnification) per subject.

Table 2 Characteristics of blank CLs and QD-CLs

Group	Zeta potential (mV)	Encapsulation efficiency (%)	Mean particle size (nm)	PDI
Blank CLs	$-(13.6 \pm 1.32)$	–	173.12	0.098
DOX-CLs	$-(16.8 \pm 1.43)$	86.3 ± 2.3	187.02	0.075
QD	$-(14.7 \pm 1.30)$	–	3.05	0.096
QD-CLs	$-(14.3 \pm 1.55)$	95.9 ± 3.1	175.26	0.090

Statistical analysis

One-way ANOVA and Student's *t* test or Kruskal–Wallis test were adopted for statistical comparison using the SAS 8.01 (1999–2000, SAS Institute Inc., Cary, NC, USA). The difference was considered to be statistically significant when the *p* value was equal or <0.05 .

Results

Characterization of DOX-CLs and QD-CLs

Physicochemical characteristics of the DOX-CLs and QD-CLs are summarized in Table 2. Microscopic images of blank CLs and QD-CLs under the white light and fluorescent light are shown in Fig. 2. Electron microscopic images demonstrated that QDs-CLs possessed uniform spherical shape (Fig. 2e). The encapsulation efficiency of QD-CLs was more than 95 %, which were consistent with the microscopic observation.

DOX-CLs also showed spherical morphology similar as QD-CLs (Fig. 2f). Dynamic light scattering results demonstrated that all CLs had average size around 180 nm in diameter. Low polydispersity index (PDI) values (<0.1) were observed in all liposomes, indicating the fairly narrow size distribution. Moderately negative zeta potential values (<-17 mV) were observed in all liposomes. The electrostatic repulsive forces provided adequate dispersion stability of CLs, as indicated by the low PDI values. The encapsulation efficiency of DOX-CLs reached 86.3 ± 2.3 %. From these results, CLs could be used as an efficient delivery system for chemotherapy.

Enhancement effects of FUS on QD-CLs cellular uptake

QD intracellular fluorescent imaging

For the tumor-targeted cell imaging study, QDs, QD-CLs, and FUS + QD-CLs were used in vitro to label C6 rat glioma cells. Red fluorescence was used to evaluate the cellular uptake of QDs by C6 cells. Among the QDs-administered groups (Fig. 3a), FUS + QD-CLs group showed the strongest fluorescent signal. However, the

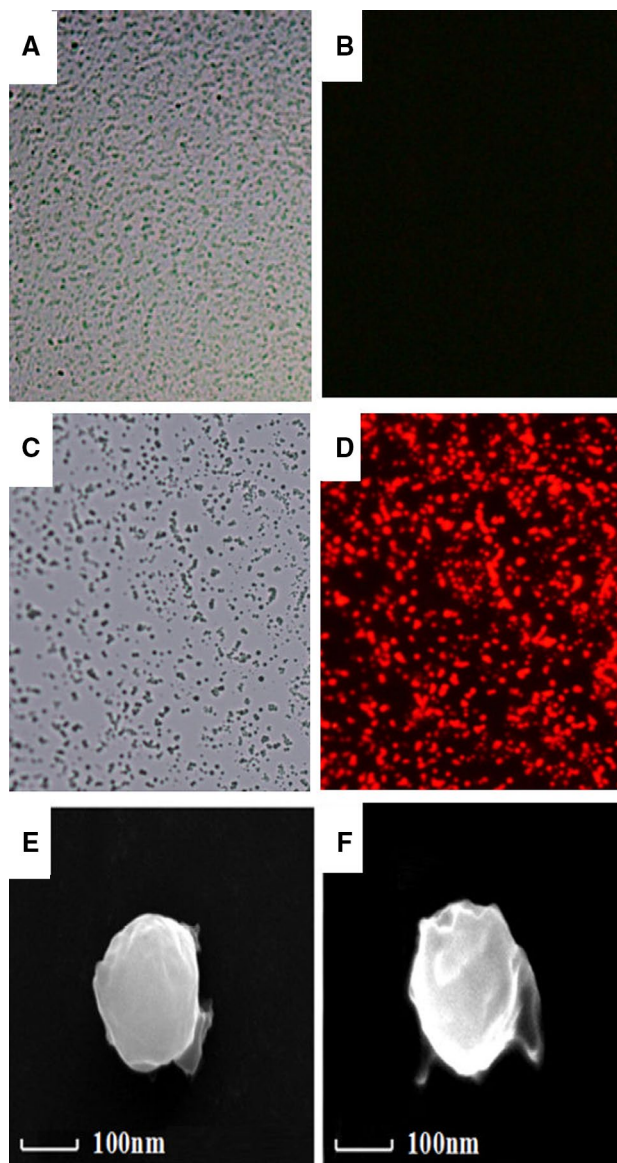


Fig. 2 Physicochemical characteristics of the DOX-CLs and QD-CLs. **a** and **b** microscopic images of blank CLs under the white light and fluorescent light, respectively (400 \times); **c** and **d** microscopic images of QD-CLs under the white light and fluorescent light, respectively (400 \times); **e** and **f** electron microscopic images of QD-CLs and DOX-CLs

fluorescent signal in QD-CLs group was a little higher than that in QDs group, especially under 50 and 100 nM QDs administration.

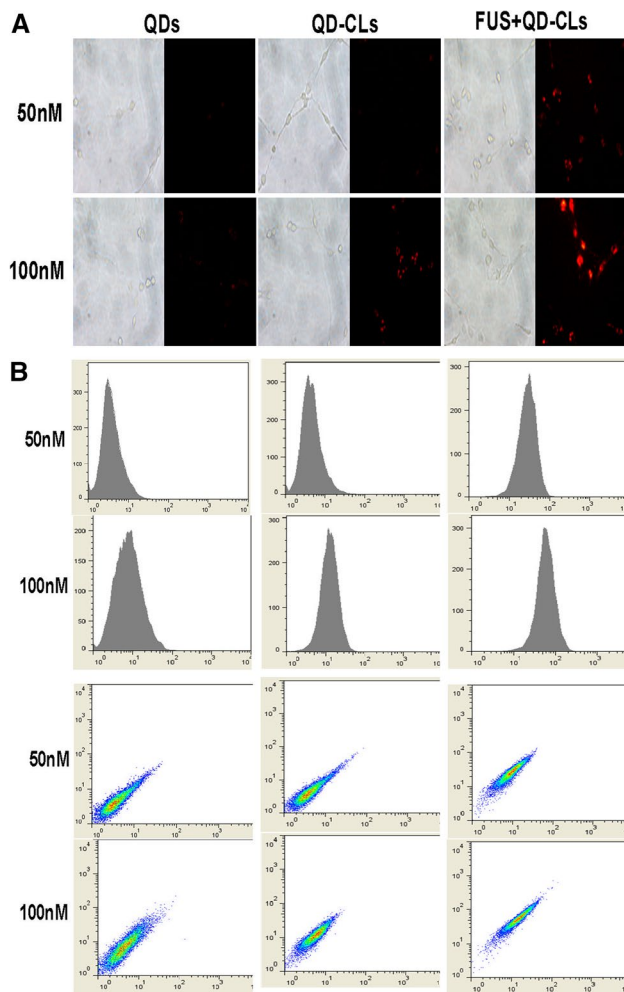


Fig. 3 Enhancement effects of FUS on QD-CLs cellular uptake. **a** Fluorescent imaging of QD intracellular under 50 and 100 nM QDs-administered groups; **b** cellular uptake of 50 and 100 nM QDs-administered groups through flow cytometry

Cellular uptake of FUS introduced QD-CLs

Cellular uptake of free QDs, QD-CLs, and FUS + QD-CLs was evaluated by flow cytometry (Fig. 3b). Among all QDs-administered groups, FUS + QD-CLs gave the strongest fluorescent signals, followed by QD group ($p < 0.01$) and QD-CLs group ($p < 0.01$). QD-CLs group produced a little shifts (right-shift indicating increased fluorescence), compared with QDs group. Meanwhile, strongest shifts were observed in FUS + QD-CLs group. These results confirmed the dual enhancement of CLs and FUS for the cellular uptake of QDs (Fig. 3a).

Glioma-targeted delivery of FUS introduced QD-CLs on rat glioma model in vivo

From experiments in vitro, intravenous QD-CLs could hardly penetrate through BBB and enter the glioma tissue

(Fig. 4a). In QD-CLs group, the glioma progression after C6 cell transplantation was hardly detected at the 7th day, but obviously observed at the 13th day. At day 25, the glioma occupied almost half of semicerebrum. However, QD-CLs group showed weak fluorescent signal in the region of glioma during the observation. In contrast, strong fluorescent signal in glioma was observed in FUS + QD-CLs group. Moreover, fluorescent signal was gradually enhanced with the glioma growth during the observation.

To confirm glioma-targeted delivery of FUS + QD-CLs, FUS + QD-CLs-treated glioma brains were fixed and sectioned after final treatment (Fig. 4b). The cell density in the mass region (Fig. 4b) was much higher than that in the contralateral normal region. Significant QDs fluorescence (red) was observed in the mass region, while little fluorescence was shown in the contralateral normal area. Combining with the FUS-mediated BBB opening technique, CLs could realize glioma-targeted delivery for chemotherapy.

Glioma-Targeted delivery of FUS introduced DOX-CLs in vitro and in vivo

Cytotoxicity of FUS + DOX-CLs on C6 glioma cells

As shown in Fig. 5a, FUS + DOX-CLs combined treatment achieved the strongest glioma inhibition effect (i.e., lowest cell viability measured by MTT assay) among all groups, followed by DOX-CLs group. In addition, FUS introduced CLs groups showed little effects on cell viability ($p > 0.05$), indicating their safety in clinical application. Overall, encapsulating DOX in CLs could effectively increase chemotherapeutic effect on glioma ($p < 0.01$), which could be further enhanced when combined with FUS technique ($p < 0.001$), and FUS alone did not cause significant change for cell viability ($p > 0.05$).

Acute toxicity of FUS introduced DOX-CLs to normal organs

Intravenous administration of FUS + DOX-CLs may cause acute toxicity to normal organs such as heart, liver, spleen, lung, and kidney. To rule out this possibility, 17.01 mg/kg DOX in DOX-CLs (20 times dosage as used in the in vivo imaging study) was given to the rats. No pathological morphology was observed in heart, liver, kidney, lung, and spleen one month after intravenous administration (Fig. 5b). Besides, all rats showed little changes in their drinking and eating behavior after treated with FUS + DOX-CLs.

Tumor volume and animal survival

To further confirm the glioma-targeted inhibition of FUS + DOX-CLs strategy, T2-weighted MRI was

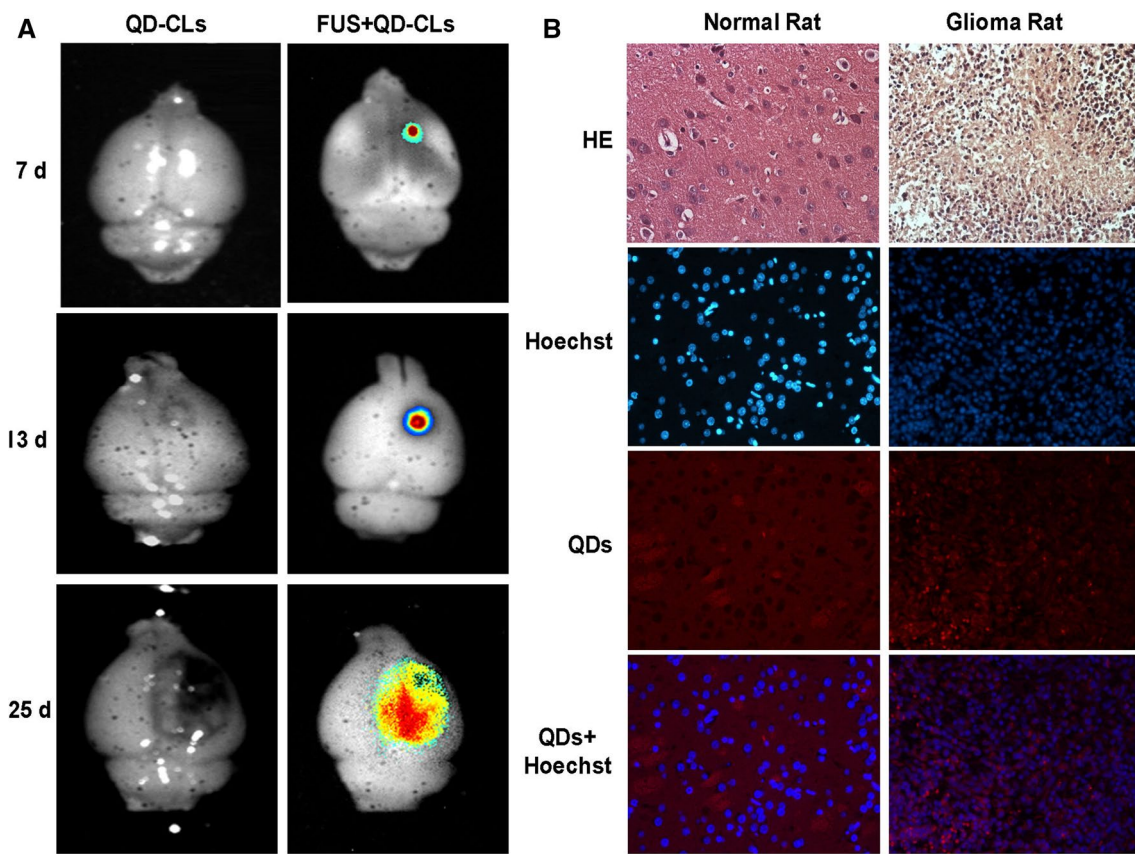


Fig. 4 Glioma-targeted delivery and effects of FUS + QD-CLs on rat glioblastoma model in vivo. **a** Fluorescent signal result of QD-CLs and FUS + QD-CLs on rat glioblastoma model; **b** fluorescent imaging of normal brain and glioma brain after FUS + QD-CLs treatment

observed in 4 weeks after treatment. As shown in Fig. 6a, FUS + DOX-CLs group showed much higher inhibition on tumor growth than other groups. Compared with the control group and FUS group, all DOX-administered groups showed enhanced animal survival (Table 3 and Supplement Fig S1). The order of the median survival days in glioma rats was FUS + DOX-CLs group > DOX-CLs group > DOX group.

HE staining and apoptosis assay (TUNEL)

From HE staining of glioma rats, gliomas in the control and FUS group showed solid mass histology that occupied a large part of brain (Fig. 6b). The tumor bulk interspersed with multiple small necrotic sites. In addition, necrotic microvessels, dilated and congested erythrocytes, were observed in glioma tissues of control and FUS group. Rapid tumor growth and invasion compressed the surrounding brain tissue, resulting in ischemia and cell death in the adjacent brain regions. Compared to the control groups, DOX group showed a reduced cellularity, with viable and dividing cells. In contrast to the control, a small cluster of recurring or residual tumor cells was found in FUS + DOX-CLs

group. Several animals in the FUS + DOX-CLs group exhibited strong treatment responses, with no tumor mass detected. Tumor in FUS + DOX-CLs group was found to be shrunken and partly destroyed comparing to its maximum size in MRI. From histological examination, all tumor tissues from the control group, FUS group, DOX group, and DOX-CLs group appeared hypercellular with obvious nuclear polymorphism. When combined with FUS, DOX-treated groups showed hypocellular tumor tissues, with high level of cell viability.

TUNEL assays were carried out to investigate the cell apoptosis in tumor tissues (Fig. 6c and Supplement Fig S2). Among all DOX-administered groups, tumor tissues from FUS + DOX-CLs group exhibited the highest level of tumor apoptosis and necrosis, indicating the enhanced chemotherapeutical effects on glioma by using DOX-CLs combined with FUS.

Discussion

Nowadays, FUS has been widely used in routine clinical diagnosis, clinical treatment, and clinical trial research.

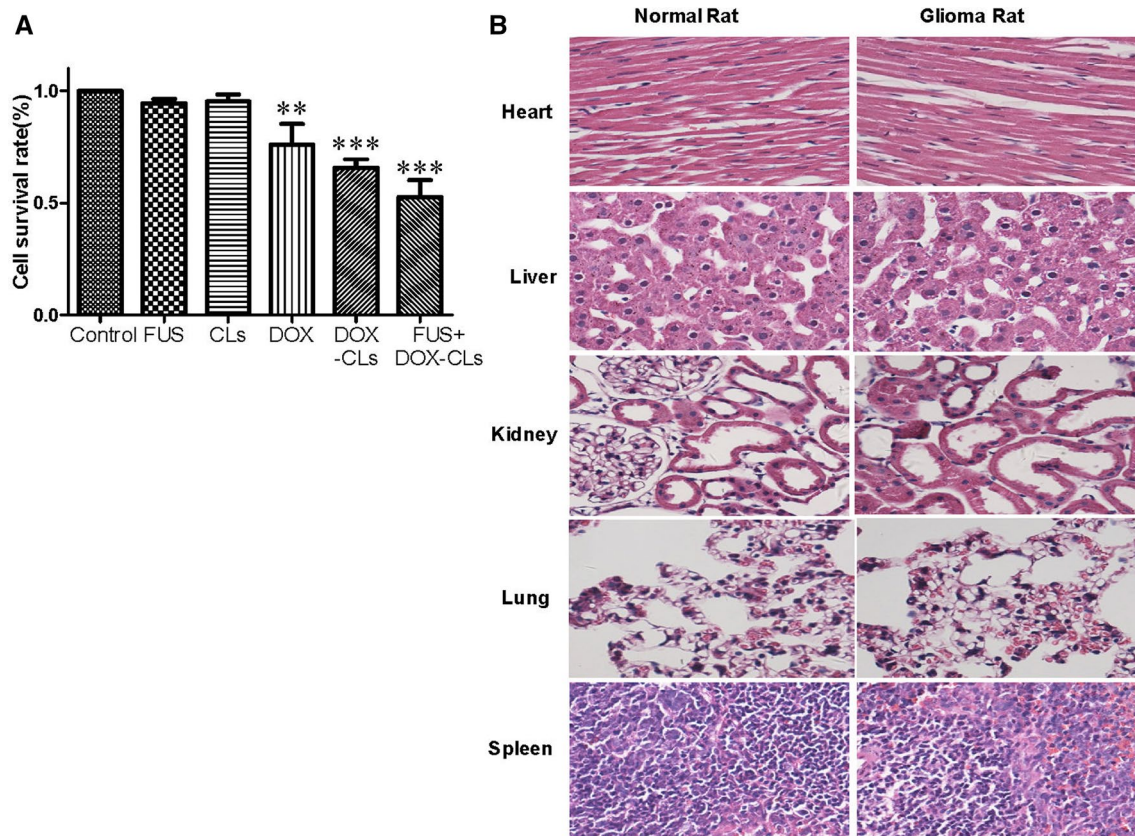


Fig. 5 Toxicity evaluation of FUS + DOX-CLs. **a** Cytotoxicity of FUS + DOX-CLs on C6 glioma cells. **b** Acute toxicity evaluation of FUS + DOX-CLs to the major organs. The HE results of heart, liver,

spleen, lung, and kidney, respectively. ** $p < 0.01$ and *** $p < 0.001$ versus control group

FUS has been reported in the treatment for osteoarthritis [26], infection and inflammation [27], fracture healing [28], thrombolysis, soft tissue repair, and antitumor therapy [29]. From recent reports, FUS can open BBB for exogenous agents [30, 31]. Meanwhile, liposome-based drug delivery system is a promising strategy to enhance the anticancer effect and reduce the cytotoxicity of chemotherapeutics [32–36]. Normally, tumor cells are characteristic of negative charge surface [28, 29], which can be used in tumor-targeted binding for chemotherapeutics. Due to their targeted and drug release functions, cationic liposomes showed the potency to increase drug efficacy in tumors [37–39]. Being hampered by BBB, a multistage targeting strategy for efficient brain tumor-targeted treatment is still needed. FUS-introduced CLs, which could improve DOX glioma-targeted delivery, were developed as a novel strategy for glioma therapy in this study. This novel treatment might offer an option for glioma chemotherapy in future clinical application.

In this study, CLs were constructed as the carriers for DOX. As shown in Table 1, DOX-CLs have suitable nanoscale size (≈ 180 nm), good polydispersity index

(PDI < 0.1), moderately negative zeta potential (-16 mV), and uniform morphology. With QDs as the tracing agent, TEM confirmed the high encapsulation efficiency of loaded CLs ($>80\%$).

The in vitro experiments confirmed the enhanced effects on glioma cell penetration by FUS introduced CLs. As shown in fluorescence imaging, FUS + QDs-CLs showed significantly higher cell uptake than those experimental groups without FUS. Similar results were observed in flow cytometer assay. These data confirmed the high efficiency of glioma-targeted delivery by FUS introduced CLs.

Brain images of glioma model rats in vivo further confirmed the glioma-targeted distribution by the multistage strategy of FUS introduced CLs. After FUS + QD-CLs administration, strong fluorescent signals were shown in the glioma region. During the observation at 7, 13, and 25 days, the fluorescent signals in FUS + QD-CLs-administered glioma tissue were enhanced with the glioma growth. The high efficient glioma-targeted delivery of FUS + QDs-CLs can be resulted from the FUS-mediated BBB opening technique and the positive binding ability of CLs on glioma. As the proposed scheme shown in Fig. 1,

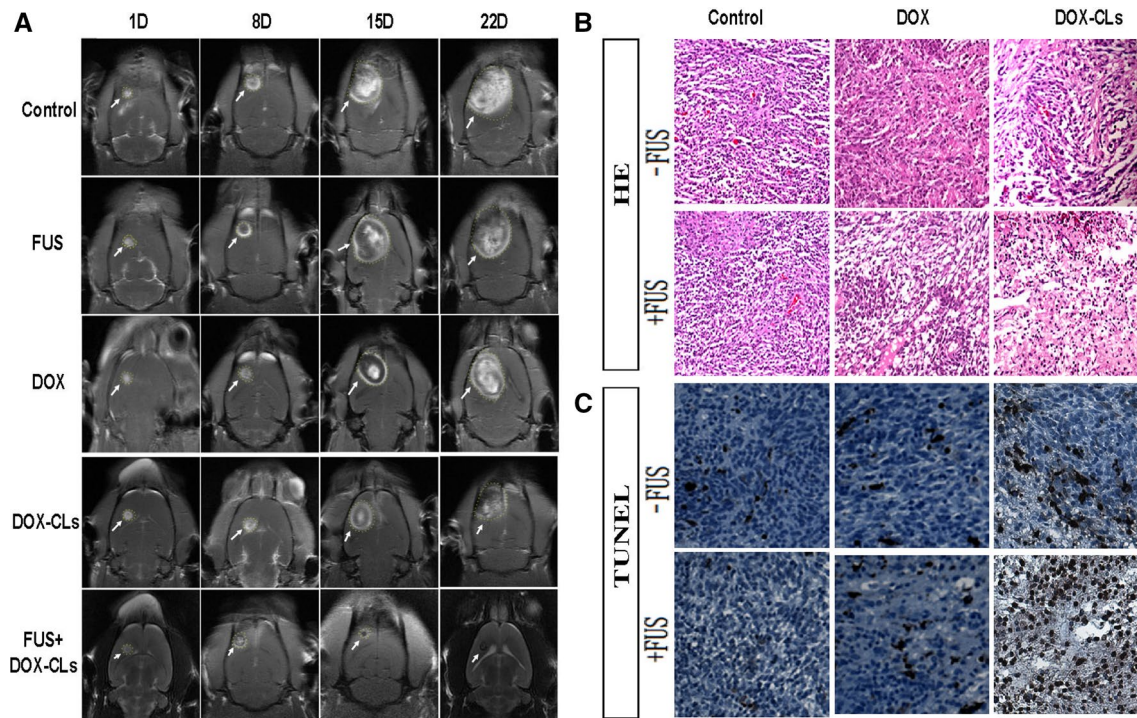


Fig. 6 Inhibition of glioma by FUS + DOX-CLs. **a** Tumor volume monitoring by MRI; **b** histology of brain tumors by HE staining; **c** glioma apoptosis assay by TUNEL

Table 3 Changes in tumor volume and animal survival time in glioma model rats after different treatment

Group	Tumor volume (mm ³)		Survival (day)
	On day 7	On day 28	
Control	10.35 ± 6.67	67.27 ± 8.63	16.5 ± 2.1
FUS	10.75 ± 5.21	55.34 ± 5.46**	22.3 ± 2.5
DOX	11.21 ± 4.98	41.56 ± 7.82***#	30.4 ± 2.9
DOX-CLs	10.78 ± 6.11	29.31 ± 4.68***#	35.0 ± 1.8
DOX-CLs + FUS	11.35 ± 4.97	11.12 ± 3.22***	81.2 ± 1.7

** $p < 0.01$ and *** $p < 0.001$ versus control group; # $p < 0.001$ versus DOX-CLs + FUS group

FUS can realize BBB opening for CLs which will complete the follow-up missions (including localize, accumulate, and retain in glioma) for loaded chemotherapeutics.

After one-month treatment, the safety of FUS + DOX-CLs on normal rats was observed. The little toxicity to heart, liver, spleen, lung, and kidney of FUS + DOX-CLs at one month could be the base safety line for FUS + DOX-CLs used in the following study. After 28-day DOX administration, FUS + DOX-CLs group showed the strongest glioma inhibition. FUS + DOX-CLs group extend the median survival to 81.2 days, followed by DOX-CLs group (35 days) and DOX group (30.4 days). From the observation of glioma histology, FUS + DOX-CLs group showed

the best cell viability among DOX-administered groups. All these data further confirmed the potential of the multistage strategy of FUS introduced CLs on glioma-targeted chemotherapy.

An anticancer treatment may lead to apoptosis of cancer cells as responses [40]. Therefore, TUNEL assay was used in this study to explore the anticancer mechanism of FUS + DOX-CLs. From the result, FUS + DOX-CLs showed the highest level of tumor apoptosis and necrosis, indicating that the enhanced chemotherapeutic effects of FUS + DOX-CLs might be resulted from the tumor cell apoptosis.

According to the present study, three advantages could be realized by this multistage targeting strategy: (1) BBB reversible opening by FUS; (2) glioma-targeted binding by CLs; and (3) prolonged glioma inhibition by FUS + DOX-CLs. With high precision to glioma tissue in brain, this novel combined strategy of FUS introduced CLs could greatly reduce the traditional dose of chemotherapeutics and diminish the likelihood of adverse systemic effects. This multistage targeting strategy could be used before or after surgery, or even in cases where surgical intervention was not feasible.

As a conclusion, the integration of nanotechnology combined with FUS may have the great potential for achieving enhanced glioma-targeted chemotherapy with minimal side effects, which might be developed as a promising and practical strategy in future clinical application.

Acknowledgments This research was supported by the National Natural Science Foundation of China (Grant Nos. 81360195, 81301982, 81571392, and 81272160), Zhejiang Provincial Natural Science Foundation of China (Grant No. LY12H31003), Zhejiang Provincial Foundation for Health Department (Grant No. 2015ZDA023), Medicine Grant from Wenzhou Bureau of Science and Technology (Grant Nos. Y2014730 and Y20140726). Major Scientific Project of Guangdong Province (Grant No. 2012A080201010). Science and Technology Program of Guangzhou, China (201508020001).

Compliance with ethical standards

Conflict of interest The authors report no conflicts of interest. The authors alone are responsible for the content and writing of this paper.

References

- Louis DN, Ohgaki H, Wiestler OD, Cavenee WK, Burger PC, Jouvet A, Scheithauer BW, Kleihues P (2007) The 2007 WHO classification of tumours of the central nervous system. *Acta Neuropathol* 114:97–109
- Schneider T, Mawrin C, Scherlach C, Skalej M, Firsching R (2010) Glioma in adults. *Dtsch Arztebl Int* 107:799–807
- Larjavaara S, Mäntylä R, Salminen T, Haapasalo H, Raitanen J, Jääskeläinen J, Auvinen A (2007) Incidence of glioma by anatomic location. *Neuro Oncol* 9:319–325
- Liu X, Cui W, Li B, Hong Z (2012) Targeted therapy for glioma using cyclic RGD-entrapped polyionic complex nanomicelles. *Int J Nanomed* 7:2853–2862
- Stan AC, Casares S, Radu D, Walter GF, Brumeanu TD (1999) Doxorubicin-induced cell death in highly invasive human gliomas. *Anticancer Res* 19:941–950
- Walter KA, Tamargo RJ, Olivi A, Burger PC, Brem H (1995) Intratumoral chemotherapy. *Neurosurgery* 37:1128–1145
- Voulgaris S, Partheni M, Karamouzis M, Dimopoulos P, Papadakis N, Kalofonos HP (2002) Intratumoral doxorubicin in patients with malignant brain gliomas. *Am J Clin Oncol* 25:60–64
- Laquintana V, Trapani A, Denora N, Wang F, Gallo JM, Trapani G (2009) New strategies to deliver anticancer drugs to brain tumors. *Expert Opin Drug Deliv* 6(10):1017–1032
- Hynynen K, McDannold N, Vykhodtseva N, Jolesz FA (2001) Noninvasive MR imaging-guided focal opening of the blood-brain barrier in rabbits. *Radiology* 220:640–646
- Choi JJ, Pernot M, Small SA, Konofagou EE (2007) Noninvasive, transcranial and localized opening of the blood-brain barrier using focused ultrasound in mice. *Ultrasound Med Biol* 33:95–104
- O'Reilly MA, Waspe AC, Ganguly M, Hynynen K (2011) Focused-ultrasound disruption of the blood-brain barrier using closely-timed short pulses: influence of sonication parameters and injection rate. *Ultrasound Med Biol* 37:587–594
- Sheikov N, McDannold N, Sharma S, Hynynen K (2008) Effect of focused ultrasound applied with an ultrasound contrast agent on the tight junctional integrity of the brain microvascular endothelium. *Ultrasound Med Biol* 34:1093–1104
- Vlachos F, Tung Y-S, Konofagou E (2011) Permeability dependence study of the focused ultrasound-induced blood-brain barrier opening at distinct pressures and microbubble diameters using DCE-MRI. *Magn Reson Med* 66:8218–8230
- Shang X, Wang P, Liu Y, Zhang Z, Xue Y (2011) Mechanism of low-frequency ultrasound in opening blood-tumor barrier by tight junction. *J Mol Neurosci* 43:364–369
- Sheikov N, McDannold N, Vykhodtseva N, Jolesz F, Hynynen K (2004) Cellular mechanisms of the blood-brain barrier opening induced by ultrasound in presence of microbubbles. *Ultrasound Med Biol* 30:979–989
- Hynynen K, Jolesz FA (1998) Demonstration of potential non-invasive ultrasound brain therapy through an intact skull. *Ultrasound Med Biol* 24:275–283
- Aubry JF, Tanter M, Pernot M, Thomas JL, Fink M (2003) Experimental demonstration of noninvasive trans-skull adaptive focusing based on prior computed tomography scans. *J Acoust Soc Am* 113:84–93
- Hynynen K, McDannold N, Clement G, Jolesz FA, Zadicario E, Killiany R, Moore T, Rosen D (2006) Preclinical testing of a phased array ultrasound system for MRI-guided noninvasive surgery of the brain—A primate study. *Eur J Radiol* 59:149–156
- Goldenberg Neil M, Steinberg Benjamin E (2010) Surface charge: a key determinant of protein localization and function. *Cancer Res* 70:1277–1280
- Hirko A, Tang F, Hughes JA (2003) Cationic lipid vectors for plasmid DNA delivery. *Curr Med Chem* 10:1185–1193
- Bally MB, Masin D, Nayar R, Cullis PR, Mayer LD (1994) Transfer of liposomal drug carriers from the blood to the peritoneal cavity of normal and ascitic tumor-bearing mice. *Cancer Chemother Pharmacol* 34:137–146
- Huang SK, Lee KD, Hong K, Friend DS, Papahadjopoulos D (1992) Microscopic localization of sterically stabilized liposomes in colon carcinoma-bearing mice. *Cancer Res* 52:5135–5143
- Huang SK, Martin FJ, Jay G, Vogel J, Papahadjopoulos D, Friend DS (1993) Extravasation and transcytosis of liposomes in Kaposi's sarcoma-like dermal lesions of transgenic mice bearing the HIV tat gene. *Am J Pathol* 143:10–14
- Jovin TM (2003) Quantum dots finally come of age. *Nat Biotechnol* 21:32–33
- Haran G, Cohen R, Bar LK, Barenholz Y (1993) Transmembrane ammonium sulfate gradients in liposomes produce efficient and stable entrapment of amphipathic weak bases. *Biochim Biophys Acta* 1151:201–215
- Golubenko TA (1991) Low-frequency ultrasound in the treatment of osteoarthritis patients. *Vopr Kurortol Fizioter Lech Fiz Kult* 2:36–39
- Serena T, Lee SK, Lam K, Attar P, Meneses P, Ennis W (2009) The impact of noncontact, nonthermal, low-frequency ultrasound on bacterial counts in experimental and chronic wounds. *Ostomy Wound Manage* 55:22–30
- Claes L, Willie B (2007) The enhancement of bone regeneration by ultrasound. *Prog Biophys Mol Biol* 93:384–398
- Behrens S, Daffertshofer M, Spiegel D, Hennerici M (1999) Low frequency, low-intensity ultrasound accelerates thrombolysis through the skull. *Ultrasound Med Biol* 25:269–273
- McDannold N, Vykhodtseva N, Hynynen K (2008) Effects of acoustic parameters and ultrasound contrast agent dose on focused-ultrasound induced blood-brain barrier disruption. *Ultrasound Med Biol* 34:930–937
- Kroll RA, Neuwelt EA (1998) Outwitting the blood-brain barrier for therapeutic purposes: osmotic opening and other means. *Neurosurgery* 42:1083–1100
- Anajafi T, Mallik S (2015) Polymersome-based drug-delivery strategies for cancer therapeutics. *Ther Deliv* 4:521–534
- Tahover E, Patil YP, Gabizon AA (2015) Emerging delivery systems to reduce doxorubicin cardiotoxicity and improve therapeutic index: focus on liposomes. *Anticancer Drugs* 26:241–258
- Itakura S, Hama S, Ohgita T, Kogure K (2014) Development of nanoparticles incorporating a novel liposomal membrane destabilization peptide for efficient release of cargos into cancer cells. *PLoS One* 9(10):111–181

35. Qu MH, Zeng RF, Fang S, Dai QS, Li HP, Long JT (2014) Liposome-based co-delivery of siRNA and docetaxel for the synergistic treatment of lung cancer. *Int J Pharm* 474:112–122
36. Gifford I, Vreeland W, Grdanovska S, Burgett E, Kalinich J, Vergara V, Wang CK, Maimon E, Poster D, Al-Sheikhly M (2014) Liposome-based delivery of a boron-containing cholesteryl ester for high-LET particle-induced damage of prostate cancer cells: a boron neutron capture therapy study. *Int J Radiat Biol* 90:480–485
37. Zheng H, Hu Y, Huang W, de Villiers S, Pentel P, Zhang J, Dorn H, Ehrich M, Zhang C (2015) Negatively charged carbon nanohorn supported cationic liposome nanoparticles: a novel delivery vehicle for anti-nicotine vaccine. *J Biomed Nanotechnol* 11(12):2197–2210
38. Tada R, Hidaka A, Iwase N, Takahashi S, Yamakita Y, Iwata T, Muto S, Sato E, Takayama N, Honjo E, Kiyono H, Kunisawa J, Aramaki Y (2015) Intranasal immunization with DOTAP cationic liposomes combined with DC-cholesterol induces potent antigen-specific mucosal and systemic immune responses in mice. *PLoS one* 10(10):e0139785
39. Dicheva BM, ten Hagen TL, Schipper D, Seynhaeve AL, van Rhoon GC, Eggermont AM, Koning GA (2014) Targeted and heat-triggered doxorubicin delivery to tumors by dual targeted cationic thermosensitive liposomes. *J Control Release* 10(195):37–48
40. Chaudhary AK, Yadav N, Bhat TA, O'Malley J, Kumar S, Chandra D (2015) A potential role of X-linked inhibitor of apoptosis protein in mitochondrial membrane permeabilization and its implication in cancer therapy. *Drug Discov Today* S1359–6446:285–288